Title

Understanding the Origin of the Nonpassivating Behavior of Si-Based Anodes during the Initial Cycles

Journal

The Journal of Physical Chemistry C, 126(33)

ISSN

1932-7447

Authors

Arca, Elisabetta
Veith, Gabriel M
Satish, Rohit
et al.

Publication Date

2022-08-25

DOI

10.1021/acs.jpcc.2c02976

Understanding the origin of the non-passivating behaviour of Si-based anodes during the initial cycles.

Elisabetta Arca[*a,†], *Gabriel M. Veith*[b], *Rohit Satish*[a], *Terri Lin*[a], *Glenn Teeter*[c], *Robert Kostecki*[*a]

a. Energy Storage and Distributed Resources, Lawrence Berkeley National Laboratory, Berkeley, California, 94720

b. Chemical Sciences Division, Oak Ridge National Laboratory, Oak Ridge Tennessee 37831.

c. Materials Science Center, National Renewable Energy Laboratory, Golden, Colorado 80401.

[†]New address: School of Mathematics, Statistics and Physics, Newcastle University, Newcastle upon Tyne, NE1 7RU, UK.

*Corresponding authors: elisabetta.arca@ncl.ac.uk; r_kostecki@lbl.gov.

Table of Contents (TOC) Graphic

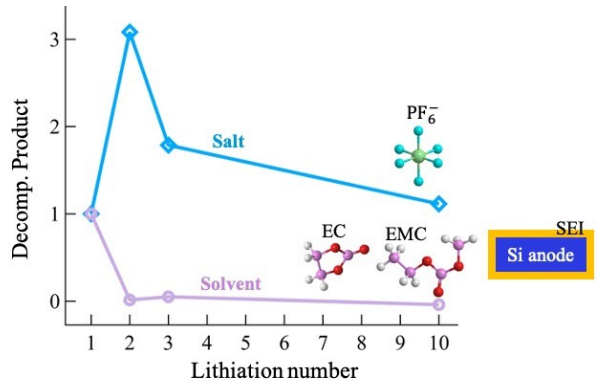

TOC sentence: The SEI on Si-anodes reduces the decomposition of the organic solvents, whereas the $LiPF_6$ salt continues to decompose upon cycling

Abstract

In this contribution, we combined electrochemical cycling and X-Ray Photoelectron Spectroscopy (XPS) to understand the non-passivating behavior of the Solid Electrolyte Interphase (SEI) on the Si anode during the first cycles. Based on galvanostatic measurements, we show that the irreversible capacity loss is reduced after the first cycle, and it stays almost constant from the second cycle onwards. XPS was used to determine the root causes of the coulombic inefficiency, showing that the rate of decomposition of the organic solvents strongly decreased after the first cycle whereas the rate of salt decomposition is almost unchanged between cycles. We determine

that the inhibition of the decomposition reaction of the organic solvent is responsible for the lower coulombic loss during the second electrochemical cycle in comparison to the first, whereas the non-passivating behavior towards the salt decomposition is one of the main causes of capacity loss upon cycling. We further revisit the role of cracking in contributing to the capacity loss. Whereas high volumetric expansion remains an issue plaguing the performance of Si-anodes, our chronoamperometry studies reveals that the SEI formed on Si anode does not passivate even when the electrode is fully expanded, and no additional surface is exposed. Overall, our work establishes the need to address the chemical and electrochemical instability of the SEI on Si anode in addition to the more notorious issue of cracking.

Introduction

The development of portable electronic devices and the electrical vehicle market has generated an increasing demand for high energy density battery materials, with enhanced volumetric and gravimetric capacity[1-6]. Silicon is widely considered as one of the most promising anode materials, due to the 10-fold higher capacity than graphite (4200 $mAhg^{-1}$ for $Li_{4.4}Si$; 3579 $mAhg^{-1}$ for $Li_{3.75}Si$ versus 372 $mAhg^{-1}$ of LiC_6)[1, 3, 6-7], its natural abundance and low cost, which make it amenable for scaling up[1-3, 6]. Despite tremendous efforts by the scientific community, battery and car manufacturers, pure silicon anodes are still far from a market reality. Increasing amounts of silicon have been introduced in composites anodes, which are still primarily made of graphite. Tesla, Varta, Sila Nanotechnologies, Enovix corporation, Gotion High-Techhave all reported improvement in the battery performance by introducing Si in composite anodes[8]. More recently Solid Power has announced commercialization of Si-reached anode (50% by weight) in an all-solid-state battery, with 80% capacity retention over hundreds of cycles[9]. Amprius claims to use 100%-Si for its anode material[10]. However, these anodes are made of silicon nanowires, a highly engineered, expensive material, whose costs are hardly sustainable for vehicles[11]. Whereas these improvements are notwithstanding, pure silicon anodes are still far from being commercialized in large scale. This is because pure Si-anodes are afflicted by rapid capacity fade and limited cycle lifetime when $LiPF_6$ in carbonate-based electrolytes is used[1-3], the extent of which is preventing its commercialization. Interestingly, the electrolyte composition used for Si anodes comprise of the same chemicals commonly used for graphite anodes [12-23] and the composition of the Solid Electrolyte Interphase (SEI) found on Si, is very similar to that reported for graphite anodes [24-26]. However, contrary to graphite anodes, the Si anodes never fully passivate, and the electrolyte continuously decomposes upon cycling[12, 16-17]. Notably, the high irreversible capacity loss during

the first cycle[27-28 29] is substantially reduced in the following cycles albeit never reaching the level of passivation required for commercial applications[27-28].

Two reasons are responsible for this non-passivating behavior: (i) the high volumetric changes upon lithium insertion and extraction, and (ii) the inherent electrochemical and chemical instability of the SEI.

The high-volume expansion and contractions with consequent mechanical fracture of electrode[1-3, 30] lead to electrode pulverization, exposing fresh Si surface at every crack, which causes electrolyte reduction[1-3]. Nano-engineering has helped mitigating the capacity fade due to mechanical problems, by tuning the Si particles size (below 150 nm)[27, 31] and their morphology[27, 31-38]. However, cycling performance and coulombic efficiency are still poor even for electrodes where nanostructuring and cycling conditions [39-42] were optimized to counteract the volume expansion. This is because the intrinsic (electro)chemical instability of the SEI is the key limiting factor. One indication of this instability is the "breathing effect", i.e., the increase and subsequent decrease of the SEI thickness upon lithiation and delithiation with every cycle[14, 16-17, 19, 43-44]. As further confirmation of this issue, we recently showed that the SEI is not stable even prior to lithiation – hence prior to cracking[45]. Indeed, in a recent prospective, Cunningham and co-authors, highlighted that the chemistry of silicon exacerbates the calendar aging issues[46] in comparison to graphite. Assessing and mitigating this shortcoming is needed to fully enable pure silicon anodes, which in turn requires to identify the causes of the inherent (electro) chemical instability of the SEI layer.

In this contribution we performed electrochemical tests coupled with post-mortem X-ray Photoelectron Spectroscopy (XPS) analysis to understand the chemical instability of the SEI. For these studies, we used 50 nm Si thin films to minimize the mechanical fracturing. Chronoamperometry tests show that the fully lithiated electrodes continuously decompose the electrolyte, at ~1$\mu A/cm^2$, when polarized at 50 mV. We hence performed X-ray Photoelectron Spectroscopy analysis to gain an understanding of what parasitic reaction are responsible for the continuous electrolyte decomposition. We determine that the decomposition rate of the solvents (EC and EMC) drastically reduces after the first cycle whereas the decomposition of the $LiPF_6$ salt continues. We attribute the strong reduction in the decomposition rate of the solvents as the main reason for the improvement in capacity retention after the first cycle, and the lack of inhibition of the salt decomposition pathways as a key-factor in the poor passivating behavior of Si-anode.

Experimental methods

Thin films of amorphous Si (50 nm) with a layer of native SiO_x (*a*-Si/*n*-SiO_x) were deposited by r.f. magnetron sputtering of intrinsic silicon (Kurt J. Lesker, 99.999%) on Cu current collector foils under argon gas at an applied power of 90 W and a throw distance of 7 cm. Electrochemical cycling was performed in a three-electrode Swagelok® cell, using 1.2M $LiPF_6$ in EC:EMC 3:7 wt. % (GEN2) as electrolyte, glass fiber (Whatman GF/D) as separator and lithium metal (Alfa Aesar, 6 mm wide, 0.75 mm thick) as counter and pseudo-reference electrode. Galvanostatic cycling were carried out on a multi-channel potentiostatic–galvanostatic (VMP3, Biologic Science Instruments, France) between 0.05 V- 1.5 V vs. Li/ Li^+ at a C/10 rate with respect to $Li_{4.4}Si$'s theoretical capacity (nominal current density of ~5 $\mu A/cm^2$) for the first 3 formation cycles, followed by 10 cycles at a C/3 rate (~16.3 $\mu A/cm^2$). Cycled electrodes were rinsed by submersion in DEC for 5 seconds prior to analysis. Thus, all data presented here are relative to the insoluble portion of the SEI. In addition, we performed chronoamperometry at the end of the 3rd lithiation and at the end of the 14th lithiation step, by holding the potential at 50 mV and recording the cathodic current.

Scanning electron microscopy (SEM) images were acquired using a JEOL JSM-6700F field emission scanning electron microscope with 5 kV accelerating voltage. X-ray Photoelectron Spectroscopy (XPS) measurements were performed using a Thermo Scientific XPS instrument operated at a base pressure better than 2×10^{-8} Torr, using an Al k-alpha source (λ = 1487 eV). In addition, extra sample reported in the supporting information were analyzed using a Kratos AXIS Nova XPS (Al k-alpha source) and PHI system (Mg k-alpha source). Curve fitting was performed using Igor Pro software with a program coded as described in Ref [47]. Phase assignment was based on the characteristic binding energy separation that chemical species presents as described in Ref [48] and Ref[45]. All data are presented as acquired, without any rescaling with respect to binding energy (BE) axis to enable analysis of possible space charge regions present at the interfaces[49-50].

Results and discussion

Electrochemical tests on the Si-anodes thin films are reported in Figure 1. First, we conducted galvanostatic cycles to determine the irreversible capacity loss during the initial formation cycles (C/10 rate) and for prolonged cycling (10 cycles at C/3 rate). The areal capacities were calculated as the mean value averaged over 4 cells. Error bars were calculated as the standard deviation of the data sets. For each cell, the irreversible capacity loss was calculated as the difference between

the lithiation and delithiation areal capacities, and the mean value was reported in Figure 1B. The error bars for the irreversible capacity loss data were calculated as the standard deviation of the data sets.

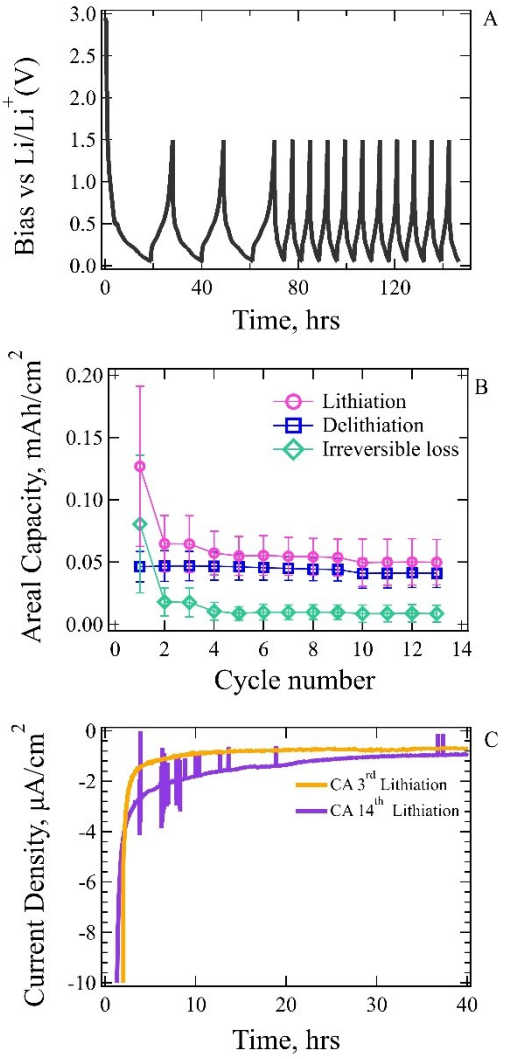

Figure 1. (A) Galvanostatic cycles, consisting of 3 initial formation cycles at a C/10 rate, followed by 10 additional cycles at C/3 rate. (B) Lithiation and Delithiation areal capacity. The difference between them represents the irreversible capacity. (C) chronoamperometry (CA) performed at the end of the 3rd lithiation step and at the end of the 14th lithiation step. Both equilibrate at ~1μA/cm^2

Figure S1 reports the discharge capacity (delithiation) for each cycle, calculated based on thickness of these films (~50nm) and the theoretical density of silicon (2.33g/cm^3). The initial capacity is ~ 4000mAhg^{-1}, very close to the theoretical value for pure silicon (4200 mAhg^{-1} for $Li_{4.4}Si$). This value decreases steadily to ~ 3500mAhg^{-1} at the end of the 13th cycle, noticing that these measurements were taken in a half-cell configuration, which uses lithium as counter electrode. As it can be seen, after the first cycle, the irreversible capacity decreases and stays

almost constant from the second cycle onwards. This means that electrolyte is getting consumed at a steady rate starting from the second cycle onwards. We note that the irreversible loss is virtually the same for both C/10 and C/3 cycling rates. This is an important result which indicates that the kinetics and mechanical issues of these films become negligible after the first cycle. Often time, particle disconnection and cracking with consequent exposure of new Si surfaces, are attributed as the root cause of this continuous electrolyte decomposition. We performed this study on 50 nm Si thin films to minimize this effect. To further prove the point, we performed SEM analysis to determine the morphology of the films upon lithiation and delithiation. The Si thin films have a granular structure already in the pristine state which does not evolve during cycling (Figure 2). We would like to emphasize that particularly at the end of the first delithiation and at the end of the second lithiation step, the SEI is extremely thin, as it can be inferred from the fact that the Si core-levels are clearly visible in Figure 3. Therefore, the SEM imagines presented in Figure 2 provide valuable information on the morphology of the underlying Si electrodes.

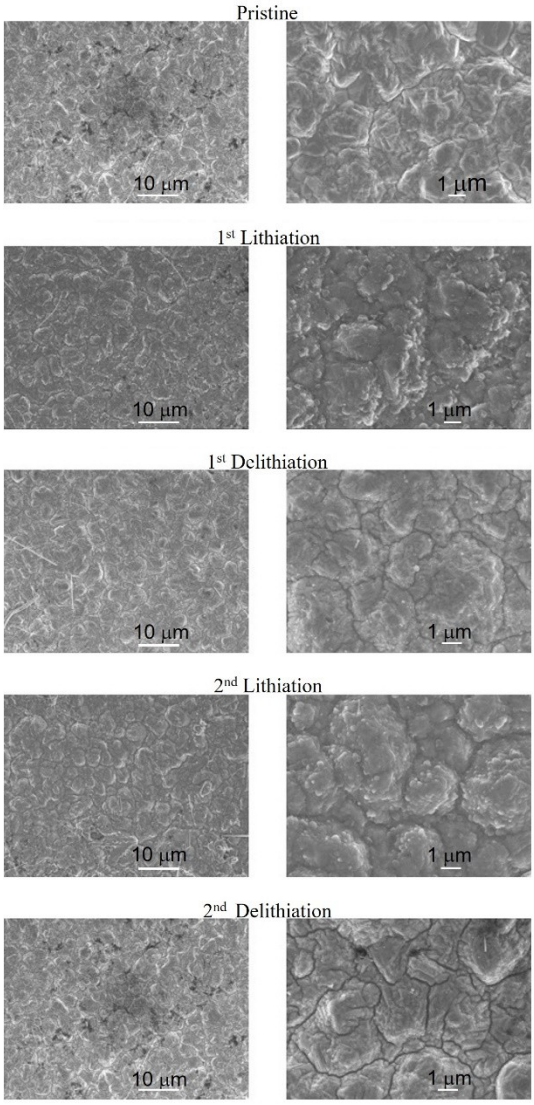

Figure 2. SEM imagines acquired after the first 2 cycles, both lithiation and delithiation steps, compared to the pristine sample.

Both the low magnification SEM imagines, and high magnification SEM imagines clearly show that there is no formation of new or additional cracks upon cycling and the granular morphology is constantly seeing throughout cycling, often defined as “dried mud” morphology. The grains become better defined upon cycling as a result of the expansion and contraction, which means they start approaching the behavior of agglomerated particles, without losing contact with the Cu counter collector. This finding seems contradictory to the general belief that capacity fading of the Si electrode is caused by the cracks. The fact that the morphology does not evolve over cycling is indicative of the fact that the Si islands generated in thin films remain attached to the Cu substrate

enabling the anode material to remain electrochemically active and withstand numerous expansion/contraction events, which is consistent with the results from other researchers. [51-53]. Dahn and co-authors have explained the process in detail for alloying anodes such as Si. For an alloy film deposited on rigid substrates, the lithiation process causes the films to expand perpendicular to the substrate. During the delithiation step, the films shrink both perpendicular and parallel to the substrates, forming a crack pattern similar to that found in dried mud. During subsequent cycles, the formed particles keep contracting and expand reversibly without further cracking. To further prove the point that the electrolyte consumption is not due to new surface being exposed, we performed chronoamperometry studies on these films. At the end of the 3rd and 14th lithiation, we perform a potentiostatic hold. We set the voltage at 50 mV, which is the lithiation cut off potential, and recorded the cathodic current for the following 40 hrs (Figure 1c). Under these conditions, the thin films are fully expanded, the surface, including any possible cracking is exposed to the electrolyte, and hence the SEI has been formed on all exposed surfaces. The sample is at its maximum volume expansion and in a steady-state conditions (no additional volume change or formation of additional cracking is possible). Under these conditions, a passivating surface would show a reduction of the cathodic current as the SEI should preclude or severely reduce any additional electrolyte decomposition. Instead, as shown in Figure 1c, a parasitic current of ~1$\mu A/cm^2$ is persistent on both cycling conditions for several hours. This is conducive of the fact that this current is consumed in parasitic reactions which are unrelated to cracking and exposure of fresh surfaces. This is the root-cause of the chemical and electrochemical non-passivating behavior of Si anodes, even for morphologies that mitigate the cracking issue through nano-engineering.

To unravel the source of these parasitic reactions, we performed qualitative and quantitative XPS analysis for the first three lithiation cycles. The high-resolution Si2p and C1s, F1s core levels are reported in Figure 3 and Figure 4 as a function of state of charges. The remaining core-levels are reported in the Supporting Information together with the tabulated peak position and quantitative analysis. Alongside information about the reactivity of the SiO_2 and Si upon lithiation, the analysis of the Si core-level provides insights into the variation of the SEI thickness upon state of charge and number of cycles (Figure 3). In an XPS experiment, the top surface is the plane of focus, thus as the SEI grows, the Si electrode is buried underneath a layer of decomposition products (SEI) and pushed outside the probing depths (~5-6 nm in the configuration adopted for this measurements). Using the intensity of the reacted silicon (silicon dioxide and silicon sub-oxides) and Si^0 peak (elemental silicon), it is possible to monitor the *average* thickness of the SEI,

bearing in mind that the SEI is not a perfectly smooth and homogenous layer, and thus local spots with thicker or thinner SEI can be present. The probing area of these XPS experiments (~ 400 μm diameter) is much larger than the local inhomogeneity (nm scale), which ensure that these local inhomogeneities do not alter the conclusion of the analysis, as the signal is averaged out over a much larger area than the characteristic size of the inhomogeneity. Further we verified the validity of the results by statistical analysis over a number of samples for any given state of charge and cycle number (at least 2 samples for each state of charge of each formation cycle). The results are presented below and both qualitative and quantitative analysis confirmed the "breathing effect", i.e., a variation in thickness and composition of the SEI over state of charges.

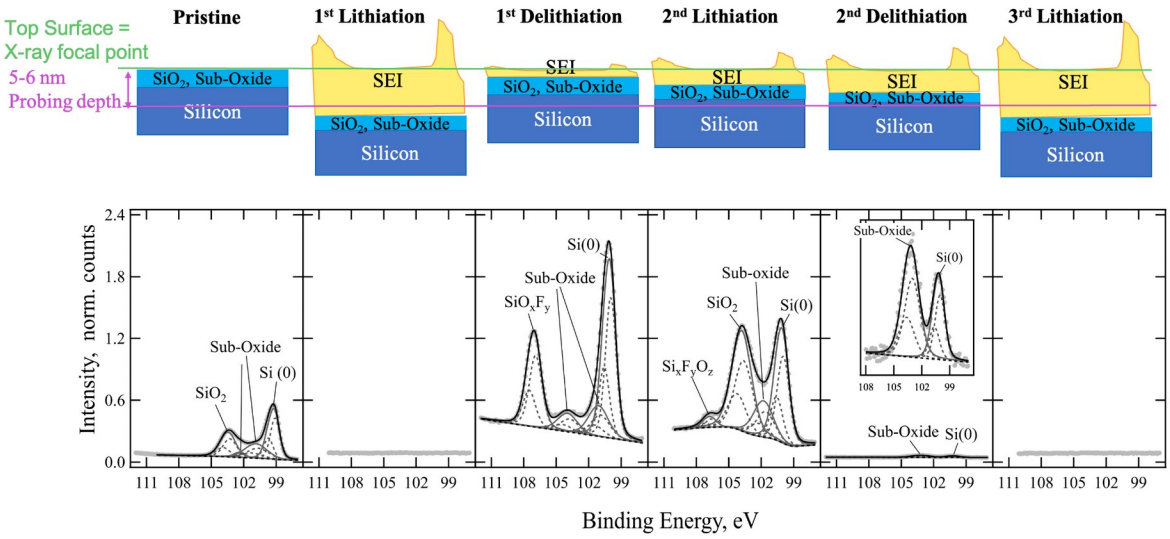

Figure 3. Growth and decrease of the SEI thickness as a function of cycle number and state of charge. The SEI grows during the lithiation stages but then it becomes thinner during the delithiation stage.

At the end of the first lithiation step, the SEI thickness exceeds the probing depth and thus the Si peak is not detectable (Figure 3). The SEI formed during the first lithiation comprises large amounts of the solvent decomposition products, most of which are carbonates[12-14, 17, 19, 54]. These can be identified unambiguously by the characteristic components on both the C (peaks labeled CO_3 and C-O-C, C-O in Figure 4). The ratio between the C-O-C, C-O and CO_3 bonds is indicative of the fact that this is a mixture of organic and inorganic carbonates. The correspondent O components (peaks labeled C=O and C-O in Figure S2) in O1s core-level, agree with the expected fingerprint for carbonate reported in literature[13-14, 17, 19, 55].

In terms of the decomposition products of the salts, LiF is again clearly and unambiguously identifiable on the F1s component (Figure 4b) and the Li1s core level at the characteristic BE separation of 629.2eV.

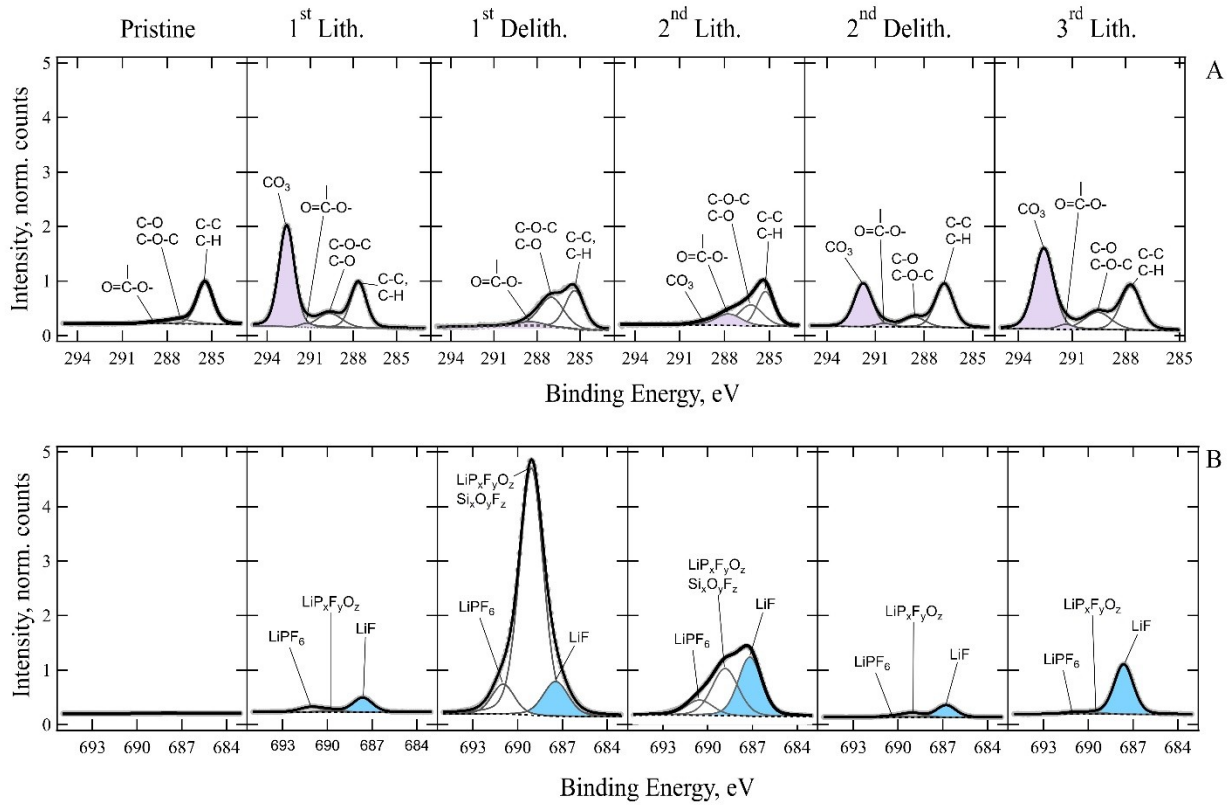

Figure 4 A) C 1s core levels as a function of the state of charge and cycle number. B) F1s core level as a function of state of charge and cycle number. Please note that all core levels have been normalized using their respective sensitivity factors for the C1s and F1s. Further peaks have been normalized to the intensity of the aliphatic carbon signal.

The F1s core-level presents (Figure 4) and P 2p (Figure S3) core levels show two additional components. These species are often attributed to $LiPF_6$ salt and $LiP_xF_yO_z$ in the literature[19, 55]. The quantitative analysis shows that the SEI is rich in the decomposition product of the solvents, with about 12.6 at.% due to C1s and 32.7% due to O1s signal of carbonate species (Figure 4 and Table S1). The salt-derived decomposition products are far less, about 3.4 at.% based on the F1s core level, of which ~2 at.% is due to LiF. This is similar to previous samples cycled in binder-free electrodes, whereas the opposite has been reported when a binder is used [28, 44].

Upon delithiation the SEI evolves significantly (Figure 3 and Figure 4). First, the thickness of the SEI strongly decreases as demonstrated by the presence of a very strong Si elemental peak. Such peaks are clearly visible also in unwashed samples, indicating that the act of delithation changes

the SEI making it weakly bound and leading to its detachment or dissolution. Specifically, the SEI thickness decreased from more than 5-6 nm at the end of the first lithiation stage, to ~2-3 nm in the delithiation stage. The latter value is determined counting $Si_xO_yF_z$ and the silica as part of the SEI. It is worth noting that the binding energy separation of the Si and O components for the fluorinated silica phase ($Si_xO_yF_z$) in this sample ($\Delta BE_{(O1s\text{-}Si2p)}$ ~ 428.2 eV) is lower than the characteristic value for SiO_2 (~ 429.5 eV) and the ratio between the two element is ~ 1:1 (instead of the 1:2 as in stoichiometric SiO_2). Furthermore, the F 1s signal shows a really intense peak at 689.1 eV, which corresponds to a mixture of fluorinated silica ($Si_xO_yF_z$) and fluorophosphates species. This is indicative that SiO_2 is not a passive spectator in the electrochemical process but, in agreement with previous reports[16, 56-57], it participates in the SEI formation and evolution. In addition, the composition of the SEI changes drastically. All carbonate species (Li_2CO_3, LiEDC etc.) are no longer present on the surface. LiF does not vary by much in comparison to the 1st lithiation stage and a small amount of lithium oxide, presumably, Li_2O_2, is present. Noticeably, the phosphorous peak undergoes a substantial transformation: a number of low binding energy components were reproducibly observed (Figure S3). In addition to $LiPF_6$ decomposition products, lower binding energies components appears. In line with a previous report[20], these components are due to phosphate species. A trace component (0.1 at.%) at binding energies ~131 eV remains unassigned.

During the second lithiation (Figure 3 and Figure 4), the thickness of the SEI grows again but to a much lower extent than the 1st lithiation. The silicon peaks are visible again for all sample measured and, for several samples, even the elemental Si(0) peak is visible. The SiO_2 continues to evolve and less fluorinated $Si_xF_yO_x$ is detected. Noticeably the composition of the SEI formed during the second lithiation is very different than the one formed during the first lithiation. A striking difference is visible in the C core level: carbonates are present in a much lower concentration if at all, with only a small number of carbon-oxygen bonds being identified in these samples. This means that the surface has been largely passivated towards the organic solvents' decomposition reactions. Conversely, the number of salt-decomposition products are present in a considerable amount. LiF is the major SEI component formed during the 2nd lithiation, with a relative at. % up to 4 times the previous samples (1st lithiation and 1st delithiation). This means that, whereas the rate of degradation of the organic solvent was strongly reduced, the rate at which the salts decompose is the same or even slightly increases during the 2nd lithiation, with LiF being one of the main decomposition products. The breathing effect continues with cycling: during the second delithiation the thickness of the SEI reduces but to a much lower extent than in the 1st

delithiation. The Si peaks are indeed far less visible in comparison to the first delithiation, because the SEI is thicker at the end of the second cycle. The composition of the SEI shows a mixture of both carbonate and fluorinated components. It is surprising to see that the carbonate components are present in quantities comparable or higher than those observed during the second lithiation step. This means that the surface has gained some level of stabilization, and possibly some of the carbonates lost during the first cycle have redeposited on the surface. The F1s signal continues to evolve accounting for most of thickness variation (breathing effect). The Si core-levels are evolving too and no signals of silica or its fluorinated version being present, only a small amount of silicon sub-oxide and elemental silicon are present. Interestingly, during the 2nd delithiation, the SEI is slightly thicker than at the of the 2nd lithiation. This is also confirmed by the reappearance of the carbonate species. Although surprising, this has been observed reproducibly, therefore over the 4 cells measured for these two states of charge, therefore washing is excluded as the source of the discrepancy. The only alternative explanation is that some species, such as the carbonate, have reach their solubility limit and they precipitate out of the solution. At the moment, this is only a hypothesis which would require further studies for confirmation.

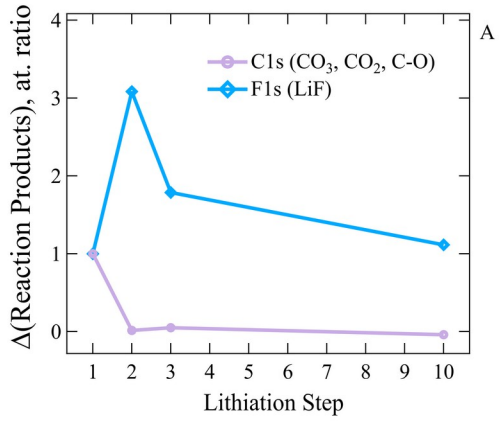

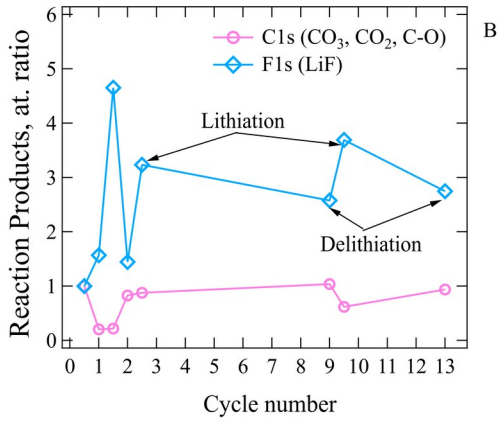

Figure 5 A) Quantification of the newly formed reaction product – Δ(Reaction Product) – at every lithiation step. Data has been normalized by the amount formed during the first lithiation step and the respective sensitivity factors. B) Quantification of the reaction product formed at every state of charge (lithiation and delithiation) for the first 13 cycles. Data has been normalized by the amount formed during the first lithiation step and the respective sensitivity factors.

During the 3rd lithiation additional decomposition of the electrolyte happens. Newly formed products accumulate on top of the decomposition products already present at the end of the second lithiation cycle, increasing the thickness of the SEI beyond the 6 nm probing depth. As a result, the Si core-levels are no longer detectable. Both carbonate or and fluorinated products are formed upon the third lithiation, with the SEI getting enriched in fluorinated products (Figure 4). This yo-yo effect continues beyond the 3rd cycle as shown in Figure 5A and B. Whereas the carbon core levels are very similar, both qualitative and quantitative for 9th lithiation and delithiation sample and the 13th delithiation sample, the composition of the F 1s core level is constantly evolving, with higher quantity of LiF for lithiated state of charges and lower quantities for delithiated state of charges (Figure 5B and supporting information Figures S5, S6 and S7).

As mentioned above, after the first lithiation step, the surface becomes partially passivated towards further electrolyte reduction. This means that either or both the decomposition reactions of solvent and salts must have slowed down, decreasing the rate at which their respective chemicals (EC, EMC and $LiPF_6$) decompose. To assess how the rate of decomposition of solvents and salt varies upon cycling, we monitor the quantity of decomposition product of the solvents and salt formed at every lithiation step and plot them as a function of lithiation number (1st, 2nd and 3rd and 10th lithiation) in Figure 5. To ensure a reliable quantification, we used atomic concentration of the CO_3, CO_2 and C-O species on the C1s core level to monitor the concentration of formed solvent decomposition product on the surface (Table S1). To determine the amount of salt decomposition product, we used the signal of the LiF on the F1s core level. There are several reasons why these species were chosen as probes of the decomposition reactions. Firstly, as illustrate above, the thickness of the SEI varies during the lithiation and delithiation steps, thus the species under examination needs to be present in the same probing depth in order for the reactions to be evaluated fairly. The SEI on both Si and graphite anodes, has been reported to be stratified, with the insoluble components (Li_2CO_3 and LiF) closer to the electrode surface and the lighter organics products accumulating in the outer parts of the SEI, closer to the bulk of electrolyte solution[16, 45, 58]. By using the CO_3, CO_2 and C-O we are considering all organic product formed. Secondly, the spectroscopic signals of these two species are clearly identifiable and they are not superimposed with the signal coming from other species (such as trace of salts such as $LiPF_6$ and

fluorophosphate), thus enabling a reliable quantification. Figure 5B shows these two quantities plotted as a function of the state of charge (lithiation and delithiation) for each cycle. Data has been normalized by the amount formed during the first lithiation step and the respective sensitivity factors. After the first cycle, decomposition products formed during any of the following lithiation steps are going to add to the SEI already present at the end of the previous delithiation step. Thus, it is important to quantify *only the newly* formed decomposition products at each lithiation step, here indicated as Δ(Reaction Products), to evaluate which of the decomposition reactions is responsible for the thickening of the SEI and the electrolyte consumption. The newly formed products, Δ(Reaction Products), have to be calculated as the difference between the amount present at a given lithiation step minus the amount present at the end of the previous delithiation step. Mathematically, this is done by subtracting the area of the relevant components at the end of the of the delithiation step, from the area of the same components at a given lithiation step. For example, the data points for the 2nd lithiation step in Figure 5A has been calculated as the normalized area of the 2nd lithiation minus the normalized area of the 1st delithiation (see Table S1 and Figure 5B). This calculation quantifies the amount of newly formed species at the 2nd lithiation step. Same calculation was performed on the 3rd lithiation with respect to the 2nd delithiation and on the 10th lithiation with respect to the 9th delithiation.

In the lithiation steps (Figure 5A), the quantity of solvent decomposition products that are newly formed upon lithiation decreased substantially from the second lithiation onwards, whereas the amount of salt decomposition products is equal or higher than those initially formed during the 1st lithiation. This is conducive of the fact that the decomposition reaction of the solvent significantly decreases upon the second lithiation, whereas the decomposition of the salt continues unabated. This phenomenon is primarily responsible for the continues consumption of the lithium inventory. In addition, the breathing effect observed for both solvent and salts decomposition products exacerbate instability of the SEI on Si-anode surfaces.

Finally, it is worth noting that a systematic trend is visible in the peak positions as function of carbonate present on the surface (Figure S8). This shift has already been reported for the SEI formed on top of graphite-based anode materials and attributed to the possible presence of a dipole at the interface between the bulk electrode and the SEI itself [50, 59]. Our data show an analogous behavior to the one reported in Ref [50]. Additionally, we note that the shift is dependent on the amount of carbonates present on the surface[52]. The physical origin of this shift is still under debate but recently it has been attributed to the orientation of the carbonate molecules[52], which if

confirmed, could explaine the observed trend with amount of carbonates species present on the surface.

Conclusions

The qualitative and quantitative analysis of the SEI formed during the first charge and discharge cycles reveal that the SEI formed on Si anodes is continuously evolving. Our study confirms the existence of a breathing process as a function of state of charge. This is visible both in terms of the thickness of the SEI and its compositions. Specifically, the thickness of the SEI grows during the lithiation steps and decreases during the delithiation steps. The most noticeable chemical species (LiF, carbonates etc.) tend to form during the lithiation process and they detach/dissolve during the delithiation process. The SiO_2 is involved in the reduction processes, giving rise to additional species such as fluorinated SiOx, and it keeps evolving during the lithiation/delithiation steps. The use of 50 nm Si electrode minimizes the possible influence of cracking effect, leaving the origin of this effect largely to the chemical and electrochemical instability of the SEI on Si. This is further confirmed by the chronoamperometry measurements: the residual cathodic current measured at the end of the 3^{rd} and 14^{th} lithiation step show that the electrolyte is continuously broken down when the electrode is polarized at 50 mV. Under these experimental conditions, the SEI is fully formed, and the electrode is fully expanded, hence no cracks can be formed anymore. A well-passivating SEI would lead to a reduction of the cathodic current to negligible values, which does not happen in Si-anode. Instead, electrolyte keeps being reduced, giving rise to a parasitic current of ~1$\mu Ah/cm^2$.

The salts decompositions reactions are a major contribution to the non-complete passivation effect observed after the first cycle, as they are not suppressed to the required extent. Whereas the rate of decomposition of the solvents is drastically reduced by about an order of magnitude after the first cycle, the decomposition of the salt continues. As a result, a carbonate-rich SEI is formed during the first lithiation, which later becomes enriched in fluorinated products during the following cycles.

Overall, our work calls for the redesign of the electrolyte for Si-anodes materials as it appears clear that traditional electrolytes used for graphite anodes lead to an unstable SEI when used on Si-anodes. One avenue could be to design larger salt than $LiPF_6$, where steric effects could limit the transport to the electrode. Alternatively, salts whose decomposition product have very limited solubility in the electrolyte itself, could be designed, to use Le Chatelier's principle to alleviate the

breathing effect plaguing the performance of Si-anodes. Recently, it was demonstrated that the addition of bulkier salts to the electrolyte composition improves the capacity retention of Si anodes[60-61]. However, the improvement is limited and not sufficient to enable commercialization of high content Si anodes. Whereas this is a promising avenue, it is these authors' opinion that additional research efforts are needed to improve the electrolyte formulation. An alternative path is to modify the electrode composition by including elements known to promote the formation of a stable SEI. As a proof of concept, we reported on the synthesis of an Al-Mn-Si based amorphous glasses[62], which shows a more stable SEI and lower parasitic currents than those observed on pure Si anodes.

Conflicts of interest

There are no conflicts to declare

Acknowledgement

This work was supported by the Assistant Secretary for Energy Efficiency and Renewable Energy, Office of Vehicle Technologies of the U.S. Department of Energy under Contract no. DE-AC02-05CH11231, under the Silicon Electrolyte Interface Stabilization (SEISta) Consortium directed by Brian Cunningham and managed by Anthony Burrell. Work at the Molecular Foundry was supported by the Office of Science, Office of Basic Energy Sciences, of the U.S. Department of Energy under Contract No. DE-AC02-05CH11231. A portion of this manuscript (films, PHI XPS, cycling - GMV) has been authored by UT-Battelle, LLC, under Contract DE-AC05-00OR22725 with the U.S. Department of Energy. We acknowledge Dr Ivana Hasa for discussion.

References

1. Wu, H.; Cui, Y., Designing Nanostructured Si Anodes for High Energy Lithium Ion Batteries. *Nano Today* **2012**, *7*, 414-429.
2. Chae, S.; Ko, M.; Kim, K.; Ahn, K.; Cho, J., Confronting Issues of the Practical Implementation of Si Anode in High-Energy Lithium-Ion Batteries. *Joule* **2017**, *1*, 47-60.
3. Jin, Y.; Zhu, B.; Lu, Z.; Liu, N.; Zhu, J., Challenges and Recent Progress in the Development of Si Anodes for Lithium-Ion Battery. *Advanced Energy Materials* **2017**, *7*, 1700715.
4. Tarascon, J. M., Key Challenges in Future Li-Battery Research. *Philosophical Transactions of the Royal Society A: Mathematical, Physical and Engineering Sciences* **2010**, *368*, 3227-3241.

5. Whittingham, M. S., Lithium Batteries and Cathode Materials. *Chemical Reviews* **2004**, *104*, 4271-4302.
6. Obrovac, M. N.; Chevrier, V. L., Alloy Negative Electrodes for Li-Ion Batteries. *Chemical Reviews* **2014**, *114*, 11444-11502.
7. Obrovac, M. N.; Christensen, L., Structural Changes in Silicon Anodes During Lithium Insertion/Extraction. *Electrochemical and Solid-State Letters* **2004**, *7*, A93-A96.
8. Fichtner, M., Recent Research and Progress in Batteries for Electric Vehicles. *Batteries & Supercaps*, *n/a*.
9. Https://Solidpowerbattery.Com/.
10. Https://Amprius.Com/.
11. Frazelle, J., Battery Day: A Closer Look at the Technology That Makes Portable Electronics Possible. *Queue* **2020**, *18*, Pages 60.
12. Jin, Y.; Kneusels, N.-J. H.; Grey, C. P., Nmr Study of the Degradation Products of Ethylene Carbonate in Silicon–Lithium Ion Batteries. *The Journal of Physical Chemistry Letters* **2019**, *10*, 6345-6350.
13. Philippe, B.; Dedryvère, R.; Allouche, J.; Lindgren, F.; Gorgoi, M.; Rensmo, H.; Gonbeau, D.; Edström, K., Nanosilicon Electrodes for Lithium-Ion Batteries: Interfacial Mechanisms Studied by Hard and Soft X-Ray Photoelectron Spectroscopy. *Chemistry of Materials* **2012**, *24*, 1107-1115.
14. Ferraresi, G.; Czornomaz, L.; Villevieille, C.; Novák, P.; El Kazzi, M., Elucidating the Surface Reactions of an Amorphous Si Thin Film as a Model Electrode for Li-Ion Batteries. *ACS Applied Materials & Interfaces* **2016**, *8*, 29791-29798.
15. Cao, C.; Steinrück, H.-G.; Shyam, B.; Stone, K. H.; Toney, M. F., In Situ Study of Silicon Electrode Lithiation with X-Ray Reflectivity. *Nano Letters* **2016**, *16*, 7394-7401.
16. Philippe, B.; Dedryvère, R.; Gorgoi, M.; Rensmo, H.; Gonbeau, D.; Edström, K., Role of the Lipf6 Salt for the Long-Term Stability of Silicon Electrodes in Li-Ion Batteries – a Photoelectron Spectroscopy Study. *Chemistry of Materials* **2013**, *25*, 394-404.
17. Radvanyi, E.; De Vito, E.; Porcher, W.; Jouanneau Si Larbi, S., An Xps/Aes Comparative Study of the Surface Behaviour of Nano-Silicon Anodes for Li-Ion Batteries. *Journal of Analytical Atomic Spectrometry* **2014**, *29*, 1120-1131.
18. Tokranov, A.; Sheldon, B. W.; Li, C.; Minne, S.; Xiao, X., In Situ Atomic Force Microscopy Study of Initial Solid Electrolyte Interphase Formation on Silicon Electrodes for Li-Ion Batteries. *ACS Applied Materials & Interfaces* **2014**, *6*, 6672-6686.
19. Veith, G. M.; Doucet, M.; Sacci, R. L.; Vacaliuc, B.; Baldwin, J. K.; Browning, J. F., Determination of the Solid Electrolyte Interphase Structure Grown on a Silicon Electrode Using a Fluoroethylene Carbonate Additive. *Scientific Reports* **2017**, *7*, 6326.
20. Xu, C.; Lindgren, F.; Philippe, B.; Gorgoi, M.; Bjorefors, F.; Edstrom, K.; Gustafsson, T., Improved Performance of the Silicon Anode for Li-Ion Batteries: Understanding the Surface Modification Mechanism of Fluoroethylene Carbonate as an Effective Electrolyte Additive. *Chemistry of Materials* **2015**, *27*, 2591-2599.
21. Nie, M. Y.; Abraham, D. P.; Chen, Y. J.; Bose, A.; Lucht, B. L., Silicon Solid Electrolyte Interphase (Sei) of Lithium Ion Battery Characterized by Microscopy and Spectroscopy. *J Phys Chem C* **2013**, *117*, 13403-13412.
22. Kundu, S.; Wang, Y. M.; Xia, W.; Muhler, M., Thermal Stability and Reducibility of Oxygen-Containing Functional Groups on Multiwalled Carbon Nanotube Surfaces: A Quantitative High-Resolution Xps and Tpd/Tpr Study. *J Phys Chem C* **2008**, *112*, 16869-16878.
23. Schroder, K. W.; Celio, H.; Webb, L. J.; Stevenson, K. J., Examining Solid Electrolyte Interphase Formation on Crystalline Silicon Electrodes: Influence of Electrochemical Preparation and Ambient Exposure Conditions. *J Phys Chem C* **2012**, *116*, 19737-19747.

24. Leroy, S.; Blanchard, F.; Dedryvere, R.; Martinez, H.; Carre, B.; Lemordant, D.; Gonbeau, D., Surface Film Formation on a Graphite Electrode in Li-Ion Batteries: Afm and Xps Study. *Surf Interface Anal* **2005**, *37*, 773-781.
25. Eshkenazi, V.; Peled, E.; Burstein, L.; Golodnitsky, D., Xps Analysis of the Sei Formed on Carbonaceous Materials. *Solid State Ionics* **2004**, *170*, 83-91.
26. Blyth, R. I. R.; Buqa, H.; Netzer, F. P.; Ramsey, M. G.; Besenhard, J. O.; Golob, P.; Winter, M., Xps Studies of Graphite Electrode Materials for Lithium Ion Batteries. *Applied Surface Science* **2000**, *167*, 99-106.
27. Graetz, J.; Ahn, C. C.; Yazami, R.; Fultz, B., Highly Reversible Lithium Storage in Nanostructured Silicon. *Electrochem Solid St* **2003**, *6*, A194-A197.
28. Michan, A. L.; Divitini, G.; Pell, A. J.; Leskes, M.; Ducati, C.; Grey, C. P., Solid Electrolyte Interphase Growth and Capacity Loss in Silicon Electrodes. *Journal of the American Chemical Society* **2016**, *138*, 7918-7931.
29. Zhu, B.; Liu, G.; Lv, G.; Mu, Y.; Zhao, Y.; Wang, Y.; Li, X.; Yao, P.; Deng, Y.; Cui, Y., et al., Minimized Lithium Trapping by Isovalent Isomorphism for High Initial Coulombic Efficiency of Silicon Anodes. *Science Advances* **2019**, *5*, eaax0651.
30. Radvanyi, E.; Porcher, W.; De Vito, E.; Montani, A.; Franger, S.; Jouanneau Si Larbi, S., Failure Mechanisms of Nano-Silicon Anodes Upon Cycling: An Electrode Porosity Evolution Model. *Physical Chemistry Chemical Physics* **2014**, *16*, 17142-17153.
31. Liu, X. H.; Zhong, L.; Huang, S.; Mao, S. X.; Zhu, T.; Huang, J. Y., Size-Dependent Fracture of Silicon Nanoparticles During Lithiation. *ACS Nano* **2012**, *6*, 1522-1531.
32. Chan, C. K.; Ruffo, R.; Hong, S. S.; Cui, Y., Surface Chemistry and Morphology of the Solid Electrolyte Interphase on Silicon Nanowire Lithium-Ion Battery Anodes. *Journal of Power Sources* **2009**, *189*, 1132-1140.
33. Chan, C. K.; Peng, H.; Liu, G.; McIlwrath, K.; Zhang, X. F.; Huggins, R. A.; Cui, Y., High-Performance Lithium Battery Anodes Using Silicon Nanowires. *Nature Nanotechnology* **2008**, *3*, 31-35.
34. Hwang, T. H.; Lee, Y. M.; Kong, B.-S.; Seo, J.-S.; Choi, J. W., Electrospun Core–Shell Fibers for Robust Silicon Nanoparticle-Based Lithium Ion Battery Anodes. *Nano Letters* **2012**, *12*, 802-807.
35. McDowell, M. T.; Lee, S. W.; Ryu, I.; Wu, H.; Nix, W. D.; Choi, J. W.; Cui, Y., Novel Size and Surface Oxide Effects in Silicon Nanowires as Lithium Battery Anodes. *Nano Letters* **2011**, *11*, 4018-4025.
36. Yao, Y.; McDowell, M. T.; Ryu, I.; Wu, H.; Liu, N.; Hu, L.; Nix, W. D.; Cui, Y., Interconnected Silicon Hollow Nanospheres for Lithium-Ion Battery Anodes with Long Cycle Life. *Nano Lett* **2011**, *11*, 2949-54.
37. Aricò, A. S.; Bruce, P.; Scrosati, B.; Tarascon, J.-M.; van Schalkwijk, W., Nanostructured Materials for Advanced Energy Conversion and Storage Devices. *Nature Materials* **2005**, *4*, 366-377.
38. Cook, J. B.; Kim, H.-S.; Lin, T. C.; Robbennolt, S.; Detsi, E.; Dunn, B. S.; Tolbert, S. H., Tuning Porosity and Surface Area in Mesoporous Silicon for Application in Li-Ion Battery Electrodes. *ACS Applied Materials & Interfaces* **2017**, *9*, 19063-19073.
39. Yoon, T.; Nguyen, C. C.; Seo, D. M.; Lucht, B. L., Capacity Fading Mechanisms of Silicon Nanoparticle Negative Electrodes for Lithium Ion Batteries. *Journal of The Electrochemical Society* **2015**, *162*, A2325-A2330.
40. Oumellal, Y.; Delpuech, N.; Mazouzi, D.; Dupré, N.; Gaubicher, J.; Moreau, P.; Soudan, P.; Lestriez, B.; Guyomard, D., The Failure Mechanism of Nano-Sized Si-Based Negative Electrodes for Lithium Ion Batteries. *Journal of Materials Chemistry* **2011**, *21*, 6201-6208.

41. Zhu, B.; Jin, Y.; Tan, Y.; Zong, L.; Hu, Y.; Chen, L.; Chen, Y.; Zhang, Q.; Zhu, J., Scalable Production of Si Nanoparticles Directly from Low Grade Sources for Lithium-Ion Battery Anode. *Nano Letters* **2015**, *15*, 5750-5754.
42. Piper, D. M.; Travis, J. J.; Young, M.; Son, S.-B.; Kim, S. C.; Oh, K. H.; George, S. M.; Ban, C.; Lee, S.-H., Reversible High-Capacity Si Nanocomposite Anodes for Lithium-Ion Batteries Enabled by Molecular Layer Deposition. *Advanced Materials* **2014**, *26*, 1596-1601.
43. Hasa, I.; Haregewoin, A. M.; Zhang, L.; Tsai, W.-Y.; Guo, J.; Veith, G. M.; Ross, P. N.; Kostecki, R., Electrochemical Reactivity and Passivation of Silicon Thin-Film Electrodes in Organic Carbonate Electrolytes. *ACS Applied Materials & Interfaces* **2020**, *12*, 40879-40890.
44. Michan, A. L.; Leskes, M.; Grey, C. P., Voltage Dependent Solid Electrolyte Interphase Formation in Silicon Electrodes: Monitoring the Formation of Organic Decomposition Products. *Chemistry of Materials* **2016**, *28*, 385-398.
45. Yin, Y.; Arca, E.; Wang, L.; Yang, G.; Schnabel, M.; Cao, L.; Xiao, C.; Zhou, H.; Liu, P.; Nanda, J., et al., Nonpassivated Silicon Anode Surface. *ACS Applied Materials & Interfaces* **2020**, *12*, 26593-26600.
46. McBrayer, J. D.; Rodrigues, M.-T. F.; Schulze, M. C.; Abraham, D. P.; Apblett, C. A.; Bloom, I.; Carroll, G. M.; Colclasure, A. M.; Fang, C.; Harrison, K. L., et al., Calendar Aging of Silicon-Containing Batteries. *Nature Energy* **2021**, *6*, 866-872.
47. Schmid, M.; Steinrück, H.-P.; Gottfried, J. M., A New Asymmetric Pseudo-Voigt Function for More Efficient Fitting of Xps Lines. *Surf Interface Anal* **2014**, *46*, 505-511.
48. Wood, K. N.; Teeter, G., Xps on Li-Battery-Related Compounds: Analysis of Inorganic Sei Phases and a Methodology for Charge Correction. *ACS Applied Energy Materials* **2018**, *1*, 4493-4504.
49. Lindgren, F.; Rehnlund, D.; Källquist, I.; Nyholm, L.; Edström, K.; Hahlin, M.; Maibach, J., Breaking Down a Complex System: Interpreting Pes Peak Positions for Cycled Li-Ion Battery Electrodes. *The Journal of Physical Chemistry C* **2017**, *121*, 27303-27312.
50. Maibach, J.; Lindgren, F.; Eriksson, H.; Edström, K.; Hahlin, M., Electric Potential Gradient at the Buried Interface between Lithium-Ion Battery Electrodes and the Sei Observed Using Photoelectron Spectroscopy. *The Journal of Physical Chemistry Letters* **2016**, *7*, 1775-1780.
51. Beaulieu, L. Y.; Eberman, K. W.; Turner, R. L.; Krause, L. J.; Dahn, J. R., Colossal Reversible Volume Changes in Lithium Alloys. *Electrochemical and Solid-State Letters* **2001**, *4*, A137.
52. Maranchi, J. P.; Hepp, A. F.; Evans, A. G.; Nuhfer, N. T.; Kumta, P. N., Interfacial Properties of the a-Si/Cu:Active–Inactive Thin-Film Anode System for Lithium-Ion Batteries. *Journal of The Electrochemical Society* **2006**, *153*, A1246.
53. Maranchi, J. P.; Hepp, A. F.; Kumta, P. N., High Capacity, Reversible Silicon Thin-Film Anodes for Lithium-Ion Batteries. *Electrochemical and Solid-State Letters* **2003**, *6*, A198.
54. Zhuang, G. V.; Xu, K.; Yang, H.; Jow, T. R.; Ross, P. N., Lithium Ethylene Dicarbonate Identified as the Primary Product of Chemical and Electrochemical Reduction of Ec in 1.2 M Lipf6/Ec:Emc Electrolyte. *The Journal of Physical Chemistry B* **2005**, *109*, 17567-17573.
55. Dedryvère, R.; Laruelle, S.; Grugeon, S.; Gireaud, L.; Tarascon, J.-M.; Gonbeau, D., Xps Identification of the Organic and Inorganic Components of the Electrode/Electrolyte Interface Formed on a Metallic Cathode. *Journal of The Electrochemical Society* **2005**, *152*, A689-A696.
56. Schnabel, M.; Harvey, S. P.; Arca, E.; Stetson, C.; Teeter, G.; Ban, C.; Stradins, P., Surface Sio2 Thickness Controls Uniform-to-Localized Transition in Lithiation of Silicon Anodes for Lithium-Ion Batteries. *ACS Applied Materials & Interfaces* **2020**, *12*, 27017-27028.

57. Schnabel, M.; Arca, E.; Ha, Y.; Stetson, C.; Teeter, G.; Han, S.-D.; Stradins, P., Enhanced Interfacial Stability of Si Anodes for Li-Ion Batteries Via Surface Sio2 Coating. *ACS Applied Energy Materials* **2020**, *3*, 8842-8849.
58. An, S. J.; Li, J.; Daniel, C.; Mohanty, D.; Nagpure, S.; Wood, D. L., The State of Understanding of the Lithium-Ion-Battery Graphite Solid Electrolyte Interphase (Sei) and Its Relationship to Formation Cycling. *Carbon* **2016**, *105*, 52-76.
59. Mozhzhukhina, N.; Flores, E.; Lundström, R.; Nyström, V.; Kitz, P. G.; Edström, K.; Berg, E. J., Direct Operando Observation of Double Layer Charging and Early Solid Electrolyte Interphase Formation in Li-Ion Battery Electrolytes. *The Journal of Physical Chemistry Letters* **2020**, *11*, 4119-4123.
60. Han, B.; Liao, C.; Dogan, F.; Trask, S. E.; Lapidus, S. H.; Vaughey, J. T.; Key, B., Using Mixed Salt Electrolytes to Stabilize Silicon Anodes for Lithium-Ion Batteries Via in Situ Formation of Li–M–Si Ternaries (M = Mg, Zn, Al, Ca). *ACS Applied Materials & Interfaces* **2019**, *11*, 29780-29790.
61. Lv, L.; Wang, Y.; Huang, W.; Wang, Y.; Zhu, G.; Zheng, H., Effect of Lithium Salt Type on Silicon Anode for Lithium-Ion Batteries. *Electrochimica Acta* **2022**, *413*, 140159.
62. Schnabel, M.; Lin, T. C.; Arca, E.; Yoon, I.; Veith, G. M.; He, X.; Kostecki, R., Stable Sei Formation on Al-Si-Mn Metallic Glass Li-Ion Anode. *Journal of The Electrochemical Society* **2021**, *168*, 100521.